2014 5th IEEE RAS & EMBS International Conference on
Biomedical Robotics and Biomechatronics (BioRob)
August 12-15, 2014. São Paulo, Brazil

Three-Dimensional Needle Steering Towards a Localized Target in a Prostate Phantom

Momen Abayazid, Navid Shahriari and Sarthak Misra

***Abstract*— Prostate biopsy and brachytherapy are commonly used for surgical interventions. In this paper, we present a three-dimensional (3D) pre-operative target localization algorithm and a real-time closed-loop control algorithm to robotically steer flexible needles with an asymmetric tip towards a real target in a prostate phantom. The phantom is composed of different tissues including rectal wall, bladder and prostate. The elasticities of these tissues are obtained using an ultrasound-based (acoustic radiation force impulse imaging) technique, and their geometry are obtained using magnetic resonance images. Six experimental cases are performed to evaluate the steering system while inserting the needle into a prostate phantom with different skin thicknesses, insertion angles and surface inclinations. The experimental results show that the target is reached by the needle in all trials. The mean targeting errors between the needle tip and the center of the target embedded in phantoms with 0 mm, 1.5 mm and 2.5 mm skin thicknesses are 1.12 mm, 0.93 mm and 0.49 mm, respectively. The variation of the insertion angle does not have an appreciable affect on the targeting accuracy. The mean targeting error during insertion into a phantom with an inclined surface is 0.85 mm. The results demonstrate the capability of proposed system to robotically steer needles towards a target for interventions in the prostate.**

I. INTRODUCTION

Percutaneous needle insertion procedures such as biopsy and brachytherapy are frequently used to detect and treat prostate cancer, respectively [1]. In both procedures, an accurate tip placement is important for successful diagnosis and treatment. The prostate is small, located within the pelvic cavity, and surrounded by critical structures, e.g., nerve bundles and blood vessels. The volume of the prostate is approximately 40 mm × 20 mm × 20 mm [2]. Thus, physicians have to carefully maneuver the needle around the critical structures in order to obtain tissue samples or deliver radioactive seeds during biopsy or brachytherapy procedures, respectively. A robotic system can aid the physicians to accurately target a suspected lesion during the procedure. Such systems require target localization, and also a control algorithm to steer the needle towards the target (lesion).

In this study, we present an ultrasound-based system that scans a soft-tissue phantom to localize the target in three-dimensional (3D)-space, and then a control algorithm is used to accurately steer the needle towards the localized target. The needle is inserted into a prostate phantom and the target is located within the prostate. Subsequently, the control algorithm can be used for steering. A method for needle control is to use its tip asymmetry (bevel tip) such as biopsy and brachytheraphy needles [3]. Such a needle deflects naturally as it is inserted into soft tissue due to asymmetric forces applied on its tip. The curvature of the needle is dependent on the stiffness of the surrounding tissue.

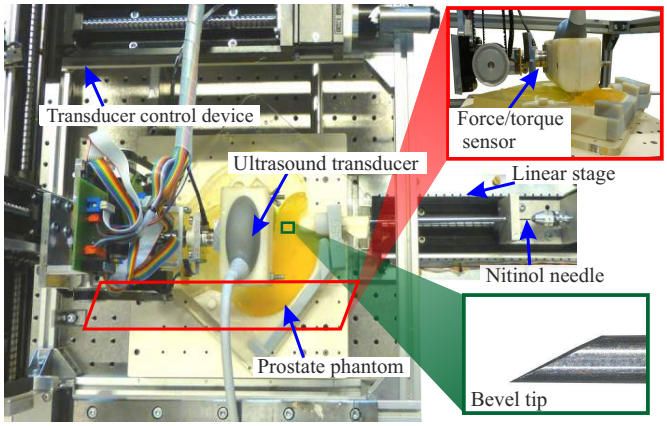

Fig. 1. The experimental setup: The setup consists of a needle insertion device to insert the bevel-tipped Nitinol needle into the soft-tissue phantom and an ultrasound control device for needle tracking. The top-right inset shows the force sensor used to keep the ultrasound probe in contact with the prostate phantom. The bottom-right inset shows the needle bevel tip.

Several research groups have used the bevel tip to steer flexible needles around obstacles in order to reach a target [4]–[6]. Webster *et al.* showed that nonholonomic kinematics of the unicycle and bicycle models can be used to predict needle path during the insertion into soft tissue [5]. Further, Abayazid *et al.* presented a two-dimensional (2D) ultrasound image-guided steering algorithm, and a 3D steering algorithm where they used both Fiber Bragg Grating sensors and ultrasound for feedback [7]–[10]. Hauser *et al.* developed a 3D feedback controller that steers the needle along a helical path, although results were evaluated in simulation without physical experiments [11].

The proposed system is a step forward to achieve a clinically-viable robotic needle steering system. The anatomical regions of interest in the patient are acquired pre-operatively using ultrasound images. A needle guide is designed to adjust the insertion angle into tissue to facilitate the procedure for the clinician. The stiffness of different tissues are determined using an ultrasound-based acoustic radiation force impulse imaging (ARFI) technique [12]. Based on the images, the clinician identifies the target location and the stiffness of the region to

The authors are affiliated with MIRA – Institute for Biomedical Technology and Technical Medicine (Robotics and Mechatronics group), University of Twente, The Netherlands. The authors would like to thank Kaj Gijsbertse for his contribution in designing the setup.
Email: {m.abayazid, n.shahriari, s.misra}@utwente.nl.
This work was supported by funds from the Netherlands Organization for Scientific Research (NWO - project:11204).

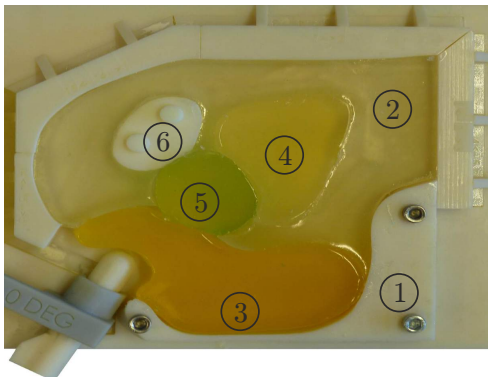

Fig. 2. The phantom that incorporates the anatomy of the male pelvic region. The anatomy is coloured for clarity. ①: Spine, ②: Adipose tissue (fat), ③: Rectal wall, ④: Urinary bladder, ⑤: Prostate and ⑥: Pubic bone.

predict the needle curvature in each region. The needle insertion procedure is autonomous under supervision of the clinician.

In the current study, we integrate the presented 3D tracking and control algorithms to steer a bevel-tipped flexible needle to reach a target in 3D space in a phantom. The phantom consists of different elasticities to mimic the properties of the tissues surrounding the target such as spine, adipose tissue, rectal wall, urinary bladder, prostate and pubic bone. This assists us to determine the effect of the tissue properties on needle deflection and the targeting accuracy during the insertion procedure. The needle is also inserted at different skin thicknesses, insertion angles and phantom inclinations to evaluate the accuracy of the steering system. The skin thickness in human ranges between 0.8 mm and 3 mm [13]. The needle guide is used to change the insertion angle. An alignment control algorithm is also developed in this study to maintain sufficient contact between the ultrasound transducer and the phantom at different surface inclinations. The alignment closed loop algorithm is based on force and torque feedback from a sensor attached to the transducer control robot (Fig. 1).

The novel aspect of our study is that we present a framework for 3D localization of the target pre-operatively. Consequently, the control algorithm steers the needle in a phantom with different skin thicknesses and elasticities, and thus different needle curvatures toward the localized target. The framework combines both target localization and control algorithms with an ultrasound-based tip tracking algorithm to steer the needle in a soft-tissue phantom with different elasticities towards a target. Such a framework can be used for intra-operative control of needle insertion during prostate interventions (biopsy and brachytherapy). In this study, magnetic resonance (MR) images are also used to develop the anatomically accurate phantom. To the best of our knowledge, the usage of known medical imaging modalities (MR and ultrasound images), and control algorithm to steer a bevel-tipped needle towards a real target in has not been investigated.

This paper is organized as follows: The experimental setup is presented in Section II. Descriptions of the control algorithm for 3D needle steering, target localization and transducer alignment are also presented in Section II. Section III describes the experimental results. Section IV concludes the results and shows directions for future work.

TABLE I

ELASTICITIES OF THE PROSTATE AND ITS SURROUNDING TISSUE. E_L REPRESENTS THE ELASTICITIES OF VARIOUS SOFT TISSUE REPORTED IN LITERATURE [14], [15]. E_{EXP} IS CALCULATED USING AN ULTRASOUND-BASED ACOUSTIC RADIATION FORCE IMPULSE IMAGING TECHNIQUE BASED ON THE SHEAR WAVE VELOCITY IN THE PHANTOM [16]. FOR THE SPINE AND PUBIC BONE, E_{EXP} IS THE ELASTICITY OF VEROWHITE–FULLCURE830.

Item # (Fig. 2)	Soft tissue	E_L (kPa)	E_{exp} (kPa)
2	Adipose tissue (fat)	10.24	10.63
3	Rectal wall	191.72	172.61
4	Urinary bladder	96.87	100.38
5	Prostate	60.50	65.89
1 and 6	Spine and pubic bone	1.82×10^6	2.50×10^3

II. METHODS

First, in Section II-A, details of the experimental setup are presented. Subsequently, in Section II-B presents the control algorithm that utilizes ultrasound images for tip tracking.

A. Experimental Setup

The experimental setup consists of a needle insertion device, an ultrasound transducer positioning device and a needle guide holder (Fig. 1). The insertion device has two degrees-of-freedom (DOFs): Translation along and rotation about the needle insertion axis [7]. On the other hand, the positioning device has three DOFs and is designed to position an ultrasound transducer in 3D space [17]. A force-torque sensor (ATI Nano-17, Industrial Automation, USA) is attached to the positioning device to measure the contact forces applied. The force measurements are used to align the transducer contact with the phantom surface to ensure having a sufficient ultrasound image quality. The guide holder is used to move the needle guide along the insertion axis. This movement of the needle guide results in the deformation of a phantom that incorporates the anatomy of the male pelvic region, i.e., prostate and surrounding structures that support it (Fig. 2). The needle is made of a Nitinol wire of 0.5 mm diameter and 30° bevel tip.

The 3D model of the phantom is developed from a series of anatomically accurate MR images and using commercial software ScanIP (Simpleware Ltd, Exeter, UK) and SolidWorks 3D Computer Aided Design (CAD) software (Dassault Systémes SolidWorks Corp., Concord, USA) [18]. Further, the phantom is made using a gelatin mixture (Dr. Oetker, Bielefeld, Germany). The compositional percentage of gelatin in the mixture is varied in order to manufacture a phantom with different elasticities.

The elasticities of the phantom are calculated using the shear wave velocity in the phantom, and also verified using dynamic mechanical analysis. Measurement of the shear wave velocity in the phantom is done using an ultrasound-based ARFI technique (Virtual Touch™ Tissue Quantification, Siemens AG Healthcare, Erlangen, Germany) [16]. The phantom is assumed to be isotropic and incompressible. Young's modulus (E) in different

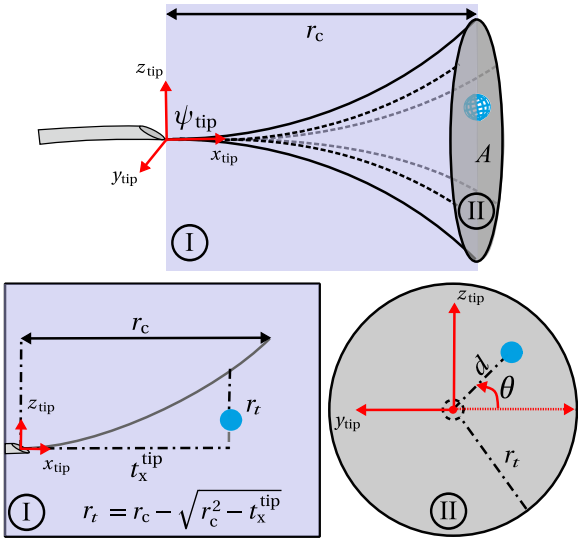

Fig. 3. Methods used for 3D needle steering. In the top figure, ψ_{tip} represents the frame attached at the tip while blue sphere represents the target. Further, r_c is defined as the radius of curvature of the circular path [5]. In inset ①, t_x^{tip} represents the distance between the plane of the control circle (plane A) and the origin of ψ_{tip}. On the other hand, r_t represents the radius of plane A. In inset ②, d and θ represents the distance of target from the center of plane A and the angle of needle rotation, respectively. In both insets ① and ②, blue circle represents the target. In inset ②, the gray circle at the center of the figure represents center of plane A.

regions is calculated as, $G = \rho v_s^2$, where G and v_s are the shear modulus and the shear wave propagation velocity, respectively [12]. The density (ρ) of the material is calculated from the mass and volume of the soft-tissue phantom and the target. Young's modulus (E) is calculated by, $E = 2G(1+\gamma)$, where γ is Poisson's ratio which is assumed to be 0.495. Siemens ACUSON S2000 system (Siemens AG, Erlangen, Germany) with a linear ultrasound transducer 18L6 is utilized to obtain ultrasound images and the transducer 9L4 is used to measure the shear wave velocity in the phantom. The spine and pubic bone (① and ⑥, Fig. 2, respectively) are made of VeroWhite - FullCure830 and printed with an Objet Eden250 3D printer (Objet Geometries Inc., Billerica, USA). Table I summarizes the elasticities calculated for the prostate and its surrounding structures (Fig. 2). The needle curvature varies during insertion into different tissue elasticities.

During needle insertion, the needle guide is pushed against the rectal wall (item ③, Fig. 2) using the needle guide holder. The control algorithm then steers the needle towards the predicted target location. The control algorithm uses ultrasound images for tip tracking. Both the control and tip tracking algorithms are described in Section II-B.

B. Needle Steering

The control algorithm for 3D needle steering estimates in real-time the region reachable by the needle. Assuming that the needle moves along a circular path during insertion [5], this region can be represented by a conical shape. Direction of the circular path depends on the bevel tip orientation, and this orientation is controlled by needle rotation about its insertion axis. This rotation enables 3D needle steering towards the target. The method used in the control algorithm is presented in Fig. 3.

The algorithm uses a frame of reference (ψ_{tip}) attached at the tip. Further, the ultrasound-based tip tracking algorithm updates in real-time the changes in the pose (position and orientation) of ψ_{tip} with respect to a global frame. The target location with respect to the needle tip ($\mathbf{p}_{tar}^{tip}$) is given by

$$\mathbf{p}_{tar}^{tip} = [t_x^{tip} \;\; t_y^{tip} \;\; t_z^{tip}]^T \tag{1}$$

where t_x^{tip}, t_y^{tip}, and t_z^{tip} are the target location along the x_{tip}–, y_{tip}–, and z_{tip}–axis, respectively. Fig. 3 shows the conical region reachable by the needle, and the plane of the control circle (plane A). Plane A is parallel to the $y_{tip}z_{tip}$–plane of ψ_{tip}, and passes through the centroid of the target.

The radius of plane A (r_t) is calculated based on the radius of curvature of the needle path (r_c) and t_x^{tip} (inset ①, Fig. 3). The radius (r_c) is obtained empirically. Experiments are performed where the needle is inserted without rotation into a soft-tissue phantom that mimics the elastic properties of the rectal wall and the prostate. The needle path is then fitted to a circular curve and its radius is determined to obtain r_c. The distance between the target and the center of plane A is given by

$$d = \sqrt{(t_y^{tip})^2 + (t_z^{tip})^2} \tag{2}$$

During insertion, r_t decreases as the needle moves towards the target. This results in the target intersecting with the circumference of plane A ($d \geq r_t$). At this instance, the needle is rotated in order to keep the needle in the reachable region. The angle of needle rotation (θ) directs the tip towards the target (inset ②, Fig. 3) and is given by

$$\theta = \tan^{-1}\left(\frac{t_z^{tip}}{t_y^{tip}}\right) \tag{3}$$

Using both the position and angle of needle rotation, the algorithm steers the needle towards the target. Additional details of the control algorithm for needle steering is presented in the work by Abayazid *et al.* [8].

The tip tracking algorithm utilizes ultrasound images obtained using the 2D transducer. Initially, the transducer is positioned perpendicular with respect to the needle insertion direction (Fig. 4). During needle insertion, this transducer is moved along the needle path using the positioning device (item ②, Fig. 4) such that the tip is always in the field-of-view of the transducer. The displacement velocity of the transducer is related to the tip velocity along the x-axis of the global frame. Tip orientation about the x-axis is obtained from the needle insertion device with an assumption that no torsion occurs along the needle shaft during insertion. Using both tip location and orientation, the pose of ψ_{tip} with respect to the global frame is deduced.

In order to improve the accuracy of the tip tracking algorithm, a closed-loop controller is used to position the transducer during needle insertion. The controller is based on the proportional-derivative algorithm and it minimizes the error between the ultrasound scanning velocity and the needle insertion velocity at its tip which

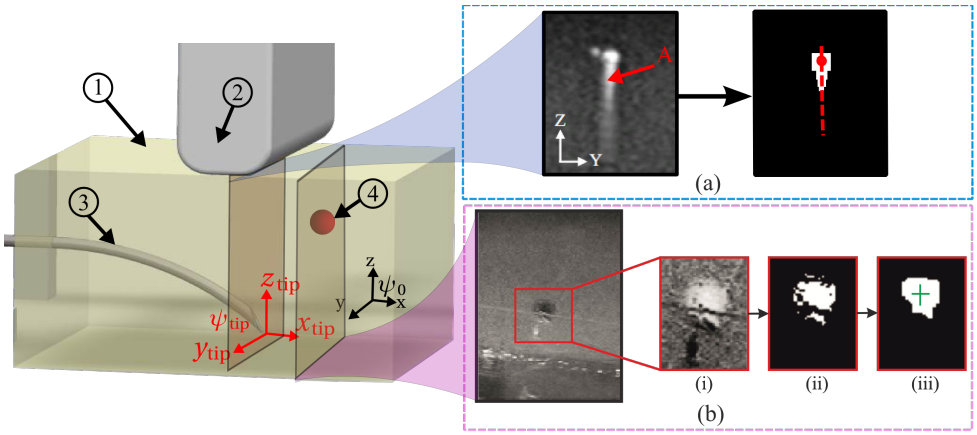

Fig. 4. A sketch of the setup for the tip tracking algorithm. ①: Phantom, ②: Transducer, ③: Needle, and ④: Target. ψ_{tip} and ψ_0 are the tip and global frames, respectively. During needle insertion, the transducer is moved along needle insertion direction such that the tip is always in the field-of-view of the transducer. (a) Ultrasound image of the tip and the comet tail artifact (A). Image processing techniques (median blur, thresholding, erosion and dilation) are applied to increase the contrast between the needle and its surrounding. Hough transform is then used to extract features of the needle and artifact. Further, the artifact has a symmetry along the red dotted line. Finally, the centroid location of the needle is shown with a red dot [17]. (b) A cropped section of the target is used for further image processing. (i) The image is inverted and the contrast is enhanced by transforming the values using contrast-limited adaptive histogram equalization. (ii) The image is converted to a binary image based on threshold. (iii) Small pixel groups are removed and the image is morphologically closed resulting in the final segmented image.

is obtained from the controller. Further, Kalman observer is also added to minimize the noise influence on the states of both tip location and velocity, and to predict the subsequent states based on the needle tip velocity [19].

Ultrasound images are also processed in real-time using basic image processing techniques such as median blur, thresholding, erosion and dilation. These techniques increase the contrast between the tip and surrounding phantom, preventing false tip detection. One point to note is that the difference in the acoustic impedance between the needle and the phantom results in a reverberation effect known as a comet tail artifact (A, Fig. 4(a)) [20]. Further, the artifact has a symmetry along a vertical center line (red dotted line, Fig. 4 (a)) and its size changes during needle insertion.

In this study, Hough Transform is used to extract features of the needle and comet tail artifact [21]. The result of the Hough transform is the series of vertical lines that describe the boundaries of the needle and comet tail artifact. By using both the symmetry property of the artifact and the set of vertical lines, the line segment that describe the symmetry line of the needle with artifact can be deduced. Subsequently, the needle centroid location along this symmetry line can be computed. Further details of the tracking algorithm is presented in the work by Vrooijink *et al.* [17]. The pose of the needle tip and hence, ψ_{tip} can be determined up to an accuracy of 0.64 mm and 2.68°.

C. Alignment control algorithm

To find the position of the target and the needle with respect to the ultrasound transducer, a pre-scan is taken and then the acquired images are processed using Matlab (v8.2, Mathworks Inc., Natick, USA). During the scan, it is essential that the ultrasound probe be kept perpendicular and in contact with the prostate phantom to acquire visible ultrasound images. As a matter of fact, we have developed a controller based on implicit force control [22], to align the transducer face with the phantom surface.

As described in Algorithm 1, where $\boldsymbol{f}_{ref}$ is the reference forces, which are all zero except for the contact direction, $\boldsymbol{f}_s$ is the force measured by the force-torque sensor, $\boldsymbol{a}$ is a constant, $\boldsymbol{K}_f$ is the controller gain, $\boldsymbol{v}_e$ is the end-effector velocity, $\boldsymbol{J}^{\dagger}$ is the pseudo-inverse of robot Jacobian and $\dot{\boldsymbol{q}}$ is the joint velocities, the alignment control is done in three steps. First, the transducer is vertically moved until it is in contact with the phantom and the contact force is equal to the reference contact force defined by the user. The force control loop is then used to minimize the force error. Finally, the transducer is moved forward in the scan direction, and again the control loop is executed. At the end of each step the ultrasound image and the transducer pose are saved as an input to the target localization algorithm.

D. Target localization

The set of ultrasound images captured during the scan are processed in order to define the target location (Fig. 4 (b)-(i)). First, each image is inverted and has its contrast enhanced by a contrast-limited adaptive histogram equalization. The images are then converted to a binary image based on a threshold value (Fig. 4 (b)-(ii)). The image is morphologically closed resulting in the segmented cross-sectional view of the target (Fig. 4 (b)-(iii)). The center of mass of this segmented target area is computed for each image using image moments and the average of all centers of mass is defined as the target center of mass. The location of the target is used as an input to the control algorithm to steer the needle towards the target.

III. Experiments

In this section, the experimental plan is described and the validation results for target localization and needle steering algorithms are presented.

A. Experimental Plan

A ϕ 0.5 mm nitinol needle with 30° bevel angle is used during all the experiments. Different experimental

Algorithm 1 Transducer alignment control during the scan

while $f_s \neq f_{ref}$ **do**
  if $f_s > f_{ref}$ **then**
    moveup()
  else
    movedown()
  end if
end while
{Starting the scan with N steps}
for $i = 0 : N$ **do**
  while $f_s < f_{ref} - a$ **or** $f_{ref} + a < f_s$ **do**
    $v_e = K_f(f_s - f_{ref})$ {End-effector velocity is defined by force error}
    $\dot{q} = J^{\dagger} v_e$ {Transform end-effector velocities to joint velocities}
    SendVelocityCommand($\dot{q}$) {send the velocity commands to the robot}
  end while
  MoveTransducer(StepSize) {move the transducer in the scan direction}
  GetUltrasoundImage() {Save the ultrasound image}
  GetTransducerPose() {Save the transducer pose}
end for

TABLE II

EXPERIMENTAL PLAN. t: SKIN THICKNESS, β: INSERTION ANGLE AND γ: SURFACE INCLINATION ANGLE OF THE PHANTOM. EACH CASE IS PERFORMED THREE TIMES.

	t (mm)			β (°)			γ (°)	
	0	**1.5**	**2.5**	**0**	**5**	**-5**	**0**	**15**
Case I	√			√			√	
Case II		√		√			√	
Case III			√	√			√	
Case IV	√				√		√	
Case V	√					√	√	
Case VI	√			√				√

scenarios are conducted to evaluate the performance of the proposed needle tracking and control algorithms. The needle radius of curvature, used as an input to the control algorithm varies depending on the tissue elasticity. The radius of curvature of the needle in the different tissues are determined empirically. The needle is inserted with a velocity of 1 mm/s and its rotational speed is 31.4 rad/s [23]. Each experimental case is performed three times. The targets are located at various locations in the prostate phantom (48-66 mm from the needle tip initial position). The needle penetrates the rectal wall (23 mm) and the prostate phantom during insertion. Before each experiment, the phantom is scanned to localize the target. The experimental cases are provided in Table II and depicted in Fig. 5.

Case I, Case II and Case III are performed to estimate the effect of skin thickness on the targeting accuracy. Silicone is used to mimic the elasticity of the skin layer (237 kPa) [24]. Case IV, Case V and Case VI evaluate the steering system with different insertion angles using the needle guide to increase the reachable region by the needle tip, and scanning phantoms with inclined surfaces.

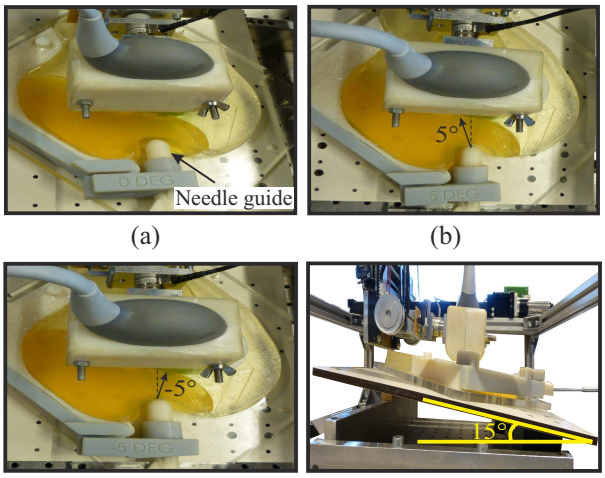

Fig. 5. In the experimental cases, the control algorithm steers the needle to reach a real target of ϕ 6 mm embedded in the prostate phantom. (a) In Case I, II and III, the needle is inserted with 5° angle into a prostate phantom with 0 mm, 1.5 mm and 2.5 mm skin thickness, respectively. (b) In Case IV, the needle is inserted with 5° angle into a prostate phantom with 0 mm skin thickness. (c) In Case V, the needle is inserted with −5° angle into a prostate phantom with 0 mm skin thickness. (d) In Case VI (side-view), the needle is inserted with 0° angle into an inclined prostate phantom (15°) with 0 mm skin.

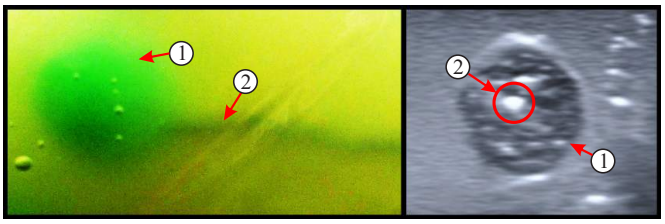

Fig. 6. The needle tip ① reaches the target ② (embedded in the prostate phantom) at the end of an insertion experiment as shown in (a) camera and (b) ultrasound images.

B. Results

The error is defined as the absolute distance between the tip and the center of the target that is localized pre-operatively. The experimental results for the six experimental cases are presented in Table III. The needle tip reaches the target in each experimental trial. Ultrasound and camera images of the needle reaching the target are shown in Fig. 6. The maximum targeting error is 1.12 mm, and it is noted in Case I. On the other hand, the minimum targeting error is 0.49 mm, and it is observed in Case III. The results show that the targeting accuracy increases as the skin thickness increases from 0 mm to 2.5 mm. The skin layer is stiffer than the other tissues in the phantom, and it supports the needle at the insertion point, and consequently, reduces needle deviation. Based on the experimental results, it is found that the effect of

TABLE III

THE RESULTS OF THE EXPERIMENTAL CASES. THE ERROR IS THE ABSOLUTE DISTANCE BETWEEN THE NEEDLE TIP AT THE END OF INSERTION AND THE CENTER OF THE LOCALIZED TARGET, WHERE THE MEAN ERROR (μ) AND STANDARD DEVIATION (σ) ARE PRESENTED IN MM.

	Case I	**Case II**	**Case III**	**Case IV**	**Case V**	**Case VI**
μ	1.12	0.93	0.49	0.64	0.75	0.85
σ	0.10	0.17	0.04	0.14	0.26	0.20

changing the insertion angle and tissue inclination does not have an appreciable effect on the targeting accuracy. *(See the accompanying video as supplementary material that demonstrates the experimental results.)*

IV. Conclusions and future work

This study combines pre-operative 3D target localization algorithm with a real-time ultrasound-based control algorithm to steer a bevel tip needle towards a real target embedded in a prostate phantom. The prostate phantom is made of different tissue elasticities (spine, adipose tissue, rectal wall, urinary bladder, prostate and pubic bone). The elasticities of these tissues are obtained using ARFI technique and their geometries are obtained using MR images. An algorithm is developed using feedback from a force-torque sensor to keep the ultrasound transducer in contact with the prostate phantom to ensure sufficient images during the insertion procedure. Six experimental cases are performed to validate the steering system using different skin thicknesses, insertion angles and inclined surfaces. The experimental results show that the mean targeting errors range between 0.49 mm and 1.12 mm. The targeting accuracy of the steering system is not drastically affected by changing the skin thickness, insertion angle and surface inclination as the target was reached during each experimental trial.

Further improvements are required to bring the system to the clinical practice. During minimally invasive interventions in the prostate, the pelvic bone may restrict the needle visibility in ultrasound images. Hence, advanced tracking algorithms using existing clinical imaging modalities need to be developed to obtain the 3D needle tip position during insertion. In future work, the ultrasound needle tracking device will be adapted to track the needle tip while scanning curved surfaces. A technique should also be developed for 3D reconstruction of the shape of targets and obstacles pre-operatively and then tracking of targets and obstacles in real-time during insertion in order to improve the targeting accuracy. The steering system can be extended to detect the patient movements that occur during needle insertion such as respiration and fluid flow. Real-time shared control between the steering algorithm and the operator will be established to achieve a practical system for clinical operations.

References

[1] T. De Silva, J. Bax, A. Fenster, J. Samarabandu, and A. D. Ward, "Quantification of prostate deformation due to needle insertion during TRUS-guided biopsy: comparison of hand-held and mechanically stabilized systems," *Medical Physics*, vol. 38, no. 3, pp. 1718–1731, March 2011.

[2] Benninghoff, *Makroskopische Anatomie, Embryologie und Histologie des Menschen.*, 1st ed. Urban und Schwarzenberg, 1993.

[3] J. Ding, D. Stoianovici, D. Petrisor, P. Mozer, R. Avila, L. Ibanez, W. Turner, D. Yankelvitz, E. Wilson, F. Banovac, and K. Cleary, "Medical needle steering for lung biopsy: Experimental results in tissue phantoms using a robotic needle driver," in *Proceedings of the 8th IEEE International Conference on BioInformatics and BioEngineering (BIBE)*, Athens, Greece, October 2008, pp. 1–5.

[4] A. M. Okamura, C. Simone, and M. D. O'Leary, "Force modeling for needle insertion into soft tissue," *IEEE Transactions on Biomedical Engineering*, vol. 51, no. 10, pp. 1707–1716, October 2004.

[5] R. J. Webster, J. S. Kim, N. J. Cowan, G. S. Chirikjian, and A. M. Okamura, "Nonholonomic modeling of needle steering," *International Journal of Robotics Research*, vol. 25, no. 5–6, pp. 509–525, May 2006.

[6] N. J. Cowan, K. Goldberg, G. S. Chirikjian, G. Fichtinger, K. B. Reed, V. Kallem, W. Park, S. Misra, and A. M. Okamura, *Surgical Robotics*. Springer US, 2011, ch. Robotic Needle Steering: Design, Modeling, Planning, and Image Guidance, pp. 557–582.

[7] M. Abayazid, R. J. Roesthuis, R. Reilink, and S. Misra, "Integrating deflection models and image feedback for real-time flexible needle steering," *IEEE Transactions on Robotics*, vol. 29, no. 2, pp. 542–553, 2013.

[8] M. Abayazid, M. Kemp, and S. Misra, "3d flexible needle steering in soft-tissue phantoms using fiber bragg grating sensors," in *Proceedings of the IEEE International Conference on Robotics and Automation (ICRA)*. Karlsruhe, Germany, May 2013, pp. 5823–5829.

[9] M. Abayazid, G. J. Vrooijink, S. Patil, R. Alterovitz, and S. Misra, "Experimental evaluation of ultrasound-guided 3d needle steering in biological tissue," *International Journal of Computer Assisted Radiology and Surgery (IJCARS)*, 2014, *In Press*, DOI:10.1007/s11548-014-0987-y.

[10] G. J. Vrooijink, M. Abayazid, S. Patil, R. Alterovitz, and S. Misra, "Needle path planning and steering in a three-dimensional non-static environment using two-dimensional ultrasound images," *International Journal of Robotics Research*, 2014, *In Press*, DOI: 10.1177/0278364914526627.

[11] K. Hauser, R. Alterovitz, N. Chentanez, A. Okamura, and K. Goldberg, "Feedback control for steering needles through 3d deformable tissue using helical paths," in *proceedings of Robotics: Science and Systems (RSS)*, vol. 37. Seattle, USA, June 2009.

[12] M. L. Palmeri, M. H. Wang, J. J. Dahl, K. D. Frinkley, and K. R. Nightingale, "Quantifying hepatic shear modulus in vivo using acoustic radiation force," *Ultrasound in medicine biology*, vol. 34, no. 4, pp. 546–558, 2008.

[13] S. Willson, E. Adam, and A. Tucker, "Patterns of breast skin thickness in normal mammograms," *Clinical Radiology*, vol. 33, no. 6, pp. 691–693, 1982.

[14] S. Misra, K. J. Macura, K. T. Ramesh, and A. M. Okamura, "The importance of organ geometry and boundary constraints for planning of medical interventions," *Medical Engineering & Physics*, vol. 31, no. 2, pp. 195–206, March 2009.

[15] Y. Hiroshi, *Strength of biological materials*, 1st ed. The Williams and Wilkins Company, 1970.

[16] A. Jahya, M. G. Schouten, J. J. Fütterer, and S. Misra, "On the importance of modelling organ geometry and boundary conditions for predicting three-dimensional prostate deformation," *Computer Methods in Biomechanics and Biomedical Engineering*, vol. 17, no. 5, pp. 497–506, 2014.

[17] G. J. Vrooijink, M. Abayazid, and S. Misra, "Real-time three-dimensional flexible needle tracking using two-dimensional ultrasound," in *Proceedings of the IEEE International Conference on Robotics and Automation (ICRA)*. Karlsruhe, Germany, May 2013, pp. 1680–1685.

[18] A. Jahya, M. Herink, and S. Misra, "A framework for predicting 3D prostate deformation in real time," *International Journal of Medical Robotics and Computer Assisted Surgery*, vol. 9, no. 4, pp. e52–e60, 2013.

[19] Y. Bar-Shalom, X. R. Li, and T. Kirubarjan, *Estimation with Applications to Tracking and Navigation*, 1st ed. John Willey and Sons, 2001.

[20] J. Huang, J. K. Triedman, N. V. Vasilyev, Y. Suematsu, R. O. Cleveland, and P. E. Dupont, "Imaging artifacts of medical instruments in ultrasound-guided interventions." *Journal of Ultrasound in Medicine*, vol. 26, no. 10, pp. 1303–1322, October 2007.

[21] S. Tsantis, G. C. Kagadis, K. Katsanos, D. Karnabatidis, G. Bourantas, and G. C. Nikiforidis, "Automatic vessel lumen segmentation and stent strut detection in intravascular optical coherence tomography." *Medical physics*, vol. 39, no. 1, pp. 503–513, January 2012.

[22] A. Visioli, G. Ziliani, and G. Legnani, "Friction compensation in hybrid force/velocity control for contour tracking tasks," *Industrial Robotics: Theory, Modeling and Control*, pp. 875–894, 2006.

[23] S. DiMaio and S. Salcudean, "Needle insertion modelling and simulation," in *Proceedings of the IEEE International Conference on Robotics and Automation (ICRA)*, vol. 2. Washington, D.C., USA, May 2002, pp. 2098–2105.

[24] M. Abayazid, J. op den Buijs, C. L. de Korte, and S. Misra, "Effect of skin thickness on target motion during needle insertion into soft-tissue phantoms," in *Proceedings of IEEE International Conference on Biomedical Robotics and Biomechatronics (BioRob)*. Rome, Italy, June 2012, pp. 755–760.